# SIMULATION OF PLANAR DEPOSITION POLYMER MELT FLOW AND FIBER ORIENTAITON IN FUSED FILAMENT FABRICATION

B. P. Heller, D. E. Smith, and D. A. Jack

Department of Mechanical Engineering, Baylor University, Waco, TX 76798

## Abstract

Mechanical and thermal properties of a 3D printed part are improved by adding discrete carbon fibers to the Fused Filament Fabrication (FFF) polymer feedstock. The properties of the fiber-filled composite are significantly influenced by the orientation of the carbon fibers within the extruded bead where fiber orientation in the bead is affected by the nozzle internal flow geometry, extrudate swell, and the deposition flow during the FFF process. In this work, a 2D Stokes flow finite element analysis is performed to evaluate FFF extrusion for a large-scale deposition extruder where special attention is given to the deposition of polymer melt on the moving platform below the nozzle. The shape of the extruded polymer is computed using a free surface normal velocity minimization technique. Once the velocity field and flow boundary is computed for the bead deposition process, fiber orientation and the resulting mechanical properties of the solidified composite are computed within the printed bead.

## Introduction

Fused Filament Fabrication (FFF) is rapidly becoming an industrially viable Additive Manufacturing (AM) technology. The ability to produce intricate three dimensional parts with minimal material waste is changing the way prototyping and small batch production is being handled. One branch of FFF that is rapidly evolving is the printing of large parts which are produced using extruders that have flow rates in the 10-100 kg/hr range and build volumes that are far larger than what can be produced with competing AM technologies.

One of the most important factors that has promoted for the advancement of large FFF structures and industrially viable parts is the addition of chopped fiber reinforcement which is added to the virgin polymers used widely in 3D printing. Specifically, chopped carbon fibers have been shown to dramatically improve the mechanical behavior of popular printing materials such as ABS [1]. Orientation of the chopped fibers following deposition affects the degree of directional improvement in mechanical properties and is therefore an important study for the understanding of part viability after production.

In previous work fiber orientation in the extrudate of an axisymmetric nozzle was evaluated by Heller, et al. [2]. This earlier work does not take into the consideration the effect of the molten polymer contacting the print plate and the velocity gradients in deposition flow which are expected to have an effect on the orientation of chopped fibers in the polymer melt. The start-stop extrudate shape of the deposition flow has been studied as well [3] using Polyflow software (ANSYS, Canonsburg, PA). The steady state deposition flow of fiber-filled polymers however has not been considered. The steady state deposition of fiber-filled polymers is assumed to represent much of the large scale deposition process. The resulting computed fiber orientation is

used here to predict the mechanical properties which are needed for structural designs and is therefore of great interest.

The orientation of discrete chopped fibers in molten polymers has been studied extensively and is well established for processes such as injection molding, compression molding, and extrusion. Early work by Jeffery [4] considered the motion of a single ellipsoid suspended in a viscous fluid undergoing simple shear flow. Folgar and Tucker [5] expanded this work using the probability density function which represents the orientation of multiple fibers, providing a means to quantify the effect of interaction among fibers within a highly concentrated suspension. The probability density function approach was improved by the Advani and Tucker [6] orientation tensor approach which served to evaluate the orientation state of the fibers using computationally efficient fiber orientation tensors. This fiber orientation evaluation method is used in mold filling programs such as Moldflow (Moldflow Corporation, Framingham, MA) and Moldex3D (Core Tech Systems Co., Ltd., Chupei City, Taiwan) which predict the fiber alignment in shear-dominated flows.

The mechanical properties of unidirectional fiber filled composites have also seen extensive study over the previous decades. Models exist for mechanical properties from Eshelby [7], Halpin-Tsai [8], Mori-Tanaka [9], or Lielens [10]. We use the approach of Tandon and Weng [11] for evaluation of the mechanical properties of unidirectional fiber filled composites. We then use the orientation homogenization method proposed by Avani and Tucker [6] and derived by Jack and Smith [12]. This method evaluates the mechanical properties of misaligned fiber filled polymer composites.

This paper presents a computational approach to evaluating the steady state flow shape of polymer deposition onto a print plate in FFF and the evaluation of the associated fiber orientation in the nozzle and in the deposited polymer bead. Our simulations evaluate the velocity gradients within the deposition flow and the related degree of orientation of the chopped fibers in the polymer melt. Expected values for mechanical properties are then computed for the fiber filled polymer after printing. Results are agreeable to similar works that have been found with extrudate shape of the deposition flow. A substantial change is seen in the fiber orientation throughout the nozzle and in the area immediately after deposition which effects the mechanical properties of the fiber filled composite.

## Methodology

### *Flow Field Evaluation*

The polymer melt flow domain which consists of the extrusion nozzle and deposited bead is created based on the geometry of the Strangpresse Model 19 large scale FFF extrusion nozzle. The extruder deposits up to 19 kgs of material per hour and is typically used during polymer deposition with a plate speed of up to $v_x$ = 4 in/s or 101.6 mm/s. Figure 1 shows the geometry of the nozzle and the boundary conditions used to compute the flow domain shape of the steady state extrudate undergoing deposition.

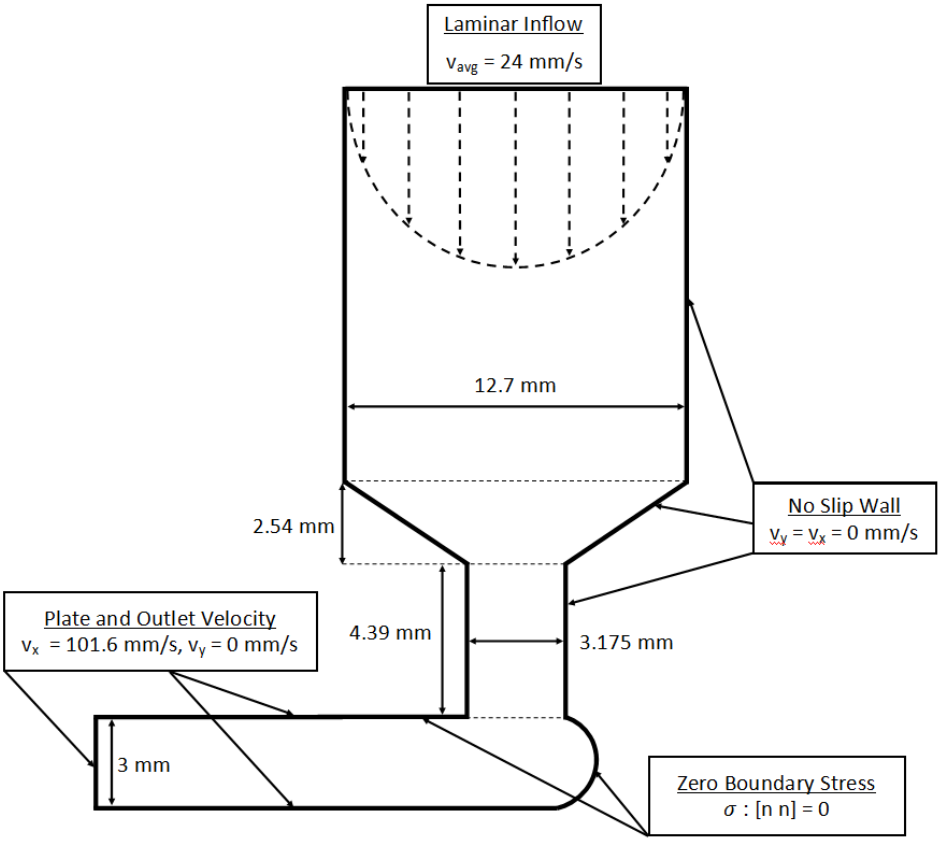


Figure 1. Nozzle Geometry Dimensions and Boundary Conditions

The fluid in our Stokes flow simulations is assumed to be a Newtonian fluid. Stokes flow is defined as

$$\nabla \cdot \mathbf{v} = 0 \tag{1}$$

and

$$\nabla \cdot \boldsymbol{\sigma} = 0 \tag{2}$$

where $\mathbf{v}$ is velocity vector and $\boldsymbol{\sigma}$ is the stress tensor given as

$$\boldsymbol{\sigma} = -p\boldsymbol{I} + \boldsymbol{\mu}[(\nabla \mathbf{v}) + (\nabla \mathbf{v})^{\mathrm{T}}] \tag{3}$$

The stress tensor is defined in terms of the pressure $p$, identity tensor $\boldsymbol{I}$, and Newtonian fluid viscosity $\boldsymbol{\mu}$. The value of viscosity in our flow simulations is 350 Pa·s which is that of ABS at a temperature of 230 °C and a shear rate of 500 $s^{-1}$, typical values in the FFF deposition process. In addition, we assume a fluid density ρ of 1040 $kg/m^3$. The outlet and plate velocities are set to $v_x$ = 4 in/s or 101.6 mm/s and $v_y$ = 0 mm/s. At this point the extruded bead is moving at a uniform velocity in the x direction with no y velocity.

The boundary conditions used for the planar deposition flow model are shown in Figure 1. The inlet of the nozzle is given as a laminar flow profile with an average velocity, $v_{avg}$ = 24 mm/s. The internal portion of the nozzle is defined as a no slip condition where $v_x$ and $v_y$ = 0 mm/s. The extrudate swell curves are defined so the boundary stress is equal to zero as

$$\boldsymbol{\sigma}:[n\,n]=0 \tag{4}$$

where " : " indicates the double contraction of the stress tensor with the normal vector giving the stress traction along the free surface.

In order to get the shape of the polymer extrudate immediately outside of the nozzle, an optimization is performed to minimize the integrated normal velocity on the leading and upper curves where the zero boundary stress condition is prescribed. The objective function for this minimization is

$$\min_{\underline{\alpha}} f(\underline{\alpha}) = \int_{S(\alpha)} \left(\underline{u}(\alpha)\cdot\underline{n}(\alpha)\right)^2 dS = 0 \tag{5}$$

where the vector $\underline{\alpha}$ contains the design variables which define the geometric location of points along the two boundary surfaces $S(\alpha)$. The square of the normal velocity along the two boundaries shown in Equation 5 is evaluated at each iteration of the minimization. We assume that the boundary surfaces to be determined by the optimization may be defined using and n[th] order Bezier curve whose recursive equation is

$$B(t) = (1-t)^n\boldsymbol{P}_0 + \binom{n}{1}(1-t)^{n-1}t\boldsymbol{P}_1 + \cdots + \binom{n}{n-1}(1-t)t^{n-1}\boldsymbol{P}_{n-1} + t^n\boldsymbol{P}_n \quad for\ t=0\to 1 \tag{6}$$

When the minimization is completed the extrudate shape in the die swell region is determined.

### *Fiber Orientation Evaluation*

Once the flow domain has been defined and the velocity field within it has been computed, the fiber orientation throughout the fluid domain can be evaluated. In our approach, streamlines are calculated within the fluid domain from which the velocity and velocity gradients $(u, v, \frac{du}{dx}, \frac{du}{dy}, \frac{dv}{dx}, \frac{dv}{dy})$ are evaluated in the flow. For this study ten evenly spaced (at the inlet) streamlines are used for the fiber orientation evaluation. The computationally efficient orientation tensor approach by Advani and Tucker [6] is used to evaluate the second order orientation tensor throughout the fluid domain through a numerical solution of

$$\frac{D\boldsymbol{A}}{Dt} = -(\boldsymbol{\Omega}\cdot\boldsymbol{A}-\boldsymbol{A}\cdot\boldsymbol{\Omega}) + \lambda(\boldsymbol{\Gamma}\cdot\boldsymbol{A}+\boldsymbol{A}\cdot\boldsymbol{\Gamma}-2\mathbb{A}:\boldsymbol{\Gamma}) + \boldsymbol{D_r} \tag{7}$$

where $\boldsymbol{A}$ and $\mathbb{A}$ are the second and fourth order orientation tensors, respectively given as

$$A_{ij} = \oint_S p_i p_j \psi(\boldsymbol{p})\, d\boldsymbol{p} \tag{8}$$

$$\mathbb{A}_{ijkl} = \oint_S p_i p_j p_k p_l \psi(\boldsymbol{p})\, d\boldsymbol{p} \tag{9}$$

In the above, $\boldsymbol{\Omega}$ is the vorticity tensor defined as

$$\boldsymbol{\Omega} = \frac{1}{2}[(\nabla\mathbf{v}) - (\nabla\mathbf{v})^{\mathrm{T}}] \tag{10}$$

and $\boldsymbol{\Gamma}$ is the rate of deformation tensor given as

$$\boldsymbol{\Gamma} = \frac{1}{2}[(\nabla \mathbf{v}) + (\nabla \mathbf{v})^{\mathrm{T}}] \tag{11}$$

The parameter $\lambda$ is related to fiber geometry as

$$\lambda = \frac{re^2 - 1}{re^2 + 1} \tag{12}$$

where $re$ is the equivalent fiber aspect ratio.

In equation 7, $\boldsymbol{D_r}$ is the fiber orientation diffusion term which accounts for fiber-fiber interactions. The Folgar-Tucker isotropic rotary diffusion (IRD) function is used in our calculations below, and is written as

$$\boldsymbol{D_r} = 2C_I\dot{\gamma}(\boldsymbol{I} - 3\boldsymbol{A}) \tag{13}$$

where $\dot{\gamma}$ is the scalar magnitude of the rate of deformation tensor defined as

$$\dot{\gamma} = (2(\boldsymbol{\Gamma}:\boldsymbol{\Gamma}))^{\frac{1}{2}} \tag{14}$$

and $C_I$ is the empirically derived interaction coefficient.

The fourth order orientation tensor, $\mathbb{A}$, in Equation 7 is needed to compute $\boldsymbol{A}$ as a function of time. Unfortuantely, the equation of motion for $\mathbb{A}$ contains the sixth-order orientation tensor (not shown), and every even ordered equation of motion contains the next higher even ordered orientation tensor. This necessitates the use of a closure whereby a higher ordered tensor is approximated as a function of lower ordered tensors. In the current study the orthotropic fitted closure (ORT) is used due to its computational stability and efficiency. The ORT closure [13,14] computes $\mathbb{A}$ from the eigenvalues $\lambda_i$, $i$ = 1,2,3, of the second order orientation tensor, $\boldsymbol{A}$, using 15 independent coefficients, as given by Verweyst [15], to obtain the approximate fourth order orientation tensor.

$$\begin{aligned}\widetilde{\mathbb{A}}_{mm}^{ORT} = \; & C_m^1 + C_m^2\lambda_1 + C_m^3\lambda_2 + C_m^4\lambda_1\lambda_2 + C_m^5\lambda_1^2 + C_m^6\lambda_1^2 + C_m^7\lambda_1^2\lambda_2 + C_m^8\lambda_1\lambda_2^2 \\ & + C_m^9\lambda_1^3 + C_m^{10}\lambda_2^3 + C_m^{11}\lambda_1^2\lambda_2^2 + C_m^{12}\lambda_1^3\lambda_2 + C_m^{13}\lambda_1\lambda_2^3 + C_m^{14}\lambda_1^4 + C_m^{15}\lambda_2^4\end{aligned} \tag{15}$$

where $\lambda_1$ and $\lambda_2$ are the eigenvalues of the second order fiber orientation tensor, and $C_m^1 - C_m^{15}$ are fitted coefficients from different flow types.

Our work quantifies fiber alignment using components of $\boldsymbol{A}$ where orientation diffusion is modeled with equation 13 and the fourth order orientation tensor closure approximation is given by equation 15. It is worth noting that an important property of $\boldsymbol{A}$ is that its trace equates to unity. It follows that a fiber orientation state for a uniformly random distribution yields a tensor $\boldsymbol{A}$ with components equal to zero except the main diagonal which has values of $\boldsymbol{A}_{ii} = 1/3$ where i = 1, 2, 3 (no summation implied). Similary, an orientation tensor $\boldsymbol{A}$ for fibers perfectly aligned in the $y$ direction would yield all diagonal components having a value of zero except $A_{22} = 1$.

We consider another approach to examine the fiber orientation state in a more general sense. This is done by taking the angle between the normal velocity vector along a streamline and the eigenvector of the maximum eigenvalue of the second order orientation tensor $\boldsymbol{A}$. The angle $\gamma$ is evaluated as

$$\gamma = \left( cos^{-1} \frac{\underline{v_n} \cdot \underline{x}^{(\lambda_m)}}{\sqrt{\underline{v_n} \cdot \underline{v_n}} \sqrt{\underline{x}^{(\lambda_m)} \cdot \underline{x}^{(\lambda_m)}}} \right) \frac{180}{\pi} \tag{16}$$

where $\underline{x}^{(\lambda_m)}$ is the eigenvector of the maximum eigenvalue of the second order orientation tensor, which defines the vector along the principal fiber direction at a point. In Equation 16, $\underline{v_n}$ is the normal velocity vector along the streamline at the same point. This evaluation method allows for an understanding of the behavior of the majority of the fibers throughout the fluid domain.

Once the fiber orientation throughout the fluid domain is computed, mechanical properties of the fiber filled polymer can be evaluated. Several models can be used to evaluate the mechanical properties of unidirectional fiber filled polymers which are summarized by Tucker and Liang [16]. The orientation homogenization method introduced by Advani and Tucker [6] and derived by Jack and Smith [12] can then be used to evaluate the elastic properties of misaligned fiber filled polymers. The orientation homogenization method used in this study is written as

$$\begin{aligned} \langle C_{ijkl} \rangle = b_1 \left( \mathbb{A}_{ijkl} \right) + b_2 \left( A_{ij} \delta_{kl} + A_{kl} \delta_{ij} \right) + b_3 \left( A_{ik} \delta_{jl} + A_{il} \delta_{jk} + A_{jl} \delta_{ik} + A_{jk} \delta_{il} \right) \\ + b_4 \left( \delta_{ij} \delta_{kl} \right) + b_5 \left( \delta_{ik} \delta_{jl} + \delta_{il} \delta_{jk} \right) \end{aligned} \tag{17}$$

where

$$b_1 = C_{11} + C_{22} - 2C_{12} - 4C_{66} \qquad b_2 = C_{12} + C_{22} \qquad b_3 = C_{66} + \frac{1}{2(C_{23} + C_{22})}$$

$$b_4 = C_{23} \qquad b_5 = \frac{1}{2(C_{22} - C_{23})} \tag{18}$$

In the above, $C_{11}$, $C_{12}$, $C_{22}$, $C_{23}$, and $C_{66}$ are the elasticity tensor coefficients of the associated unidirectional short fiber composite. In this study, these coefficients are calculated using the Tandon-Weng [11] approach.

## Results

### *Flow Modeling Results*

The results using the minimization approach to find the extrudate shape in deposition flow are shown in Figures 1-5. In Figure 1, the initial guess for the minimization is shown where the design variables for the upper curve are y values set as 3 mm and the design variables for the lower curve are x values set as 3 mm respectively. This initial guess yields an objective function value of 458.4 $mm^2/s^2$.

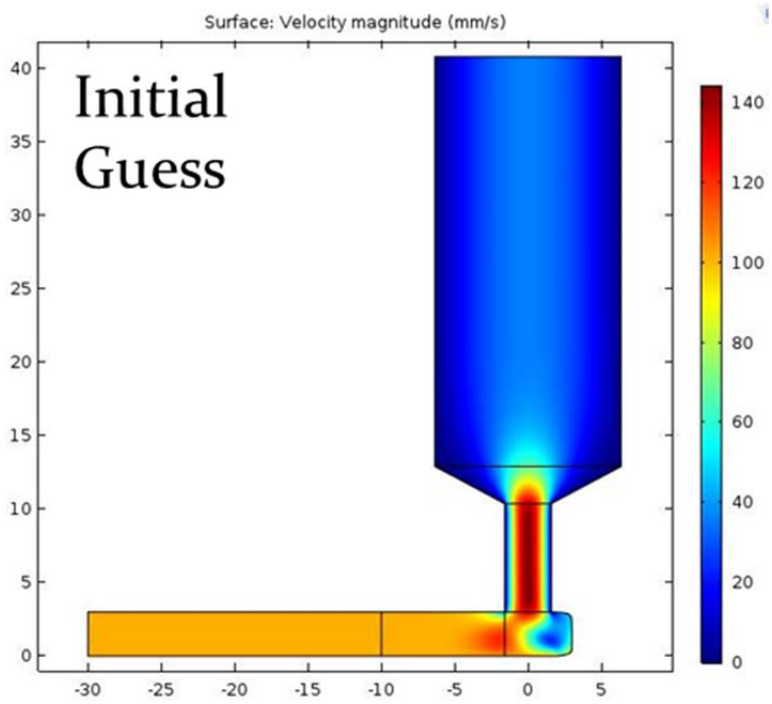

Figure 1. Initial Guess for Minimization

In Figure 2. the minimization history is shown with the value of the objective function as a function of iteration number. Note that the objective function value decreases from 458.4 $mm^2/s^2$ to 1.6 $mm^2/s^2$ over 51 iterations, which is a reduction in objective function value of 99.7%.

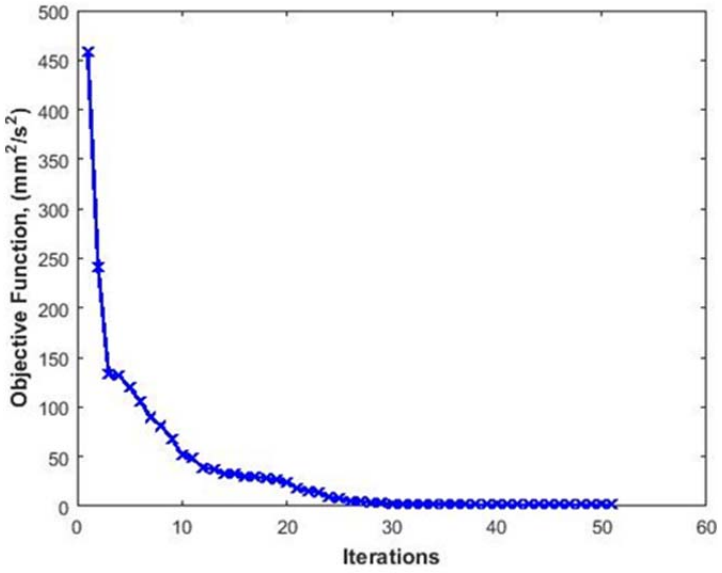

Figure 2. Objective Function Value with Respect to Iteration Number

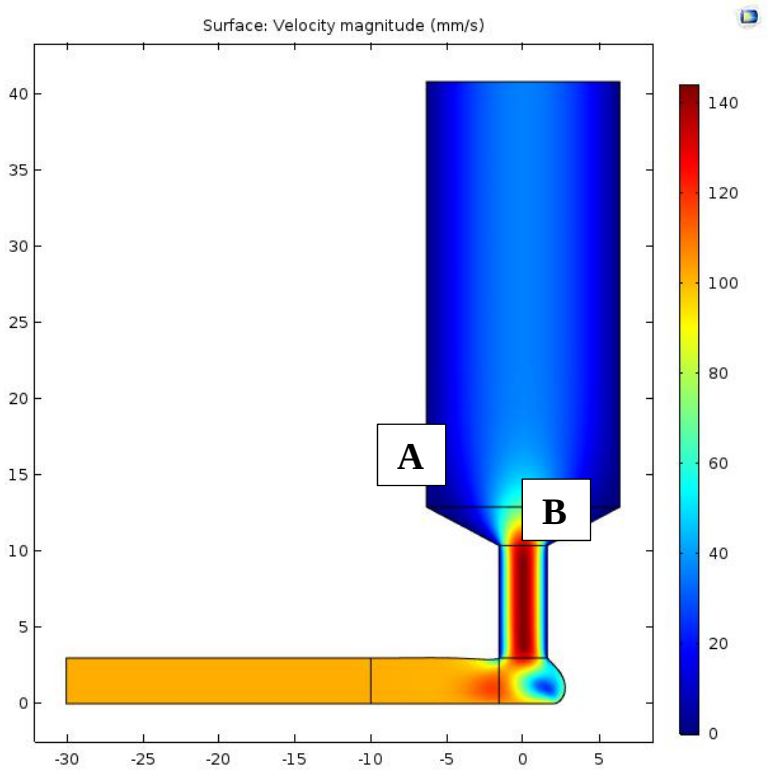

Figure 3. Optimized Deposition Flow Shape

It is seen that the optimum shape of the deposition appearing in Figure 3 has a non-zero value for the objective function. This is due to the inherent singularities that occur at a no slip to free surface boundary condition point. The singularities that effect the value of the objective function are shown in Figures 4 and 5 (labeled as A and B for clarity). It is seen that except at the endpoints, where large thin peaks exist, the values of velocity normal to the extrudate surface are nearly zero. These non-zero peaks add a small value to the objective function in the minimization. Notice also that in Figure 4, which represents the upper minimization curve, there is a peak at each end. This is due to a very small difference in the velocity components at the change in boundary condition but also notice that the magnitude of this peak is on the order of 0.36.

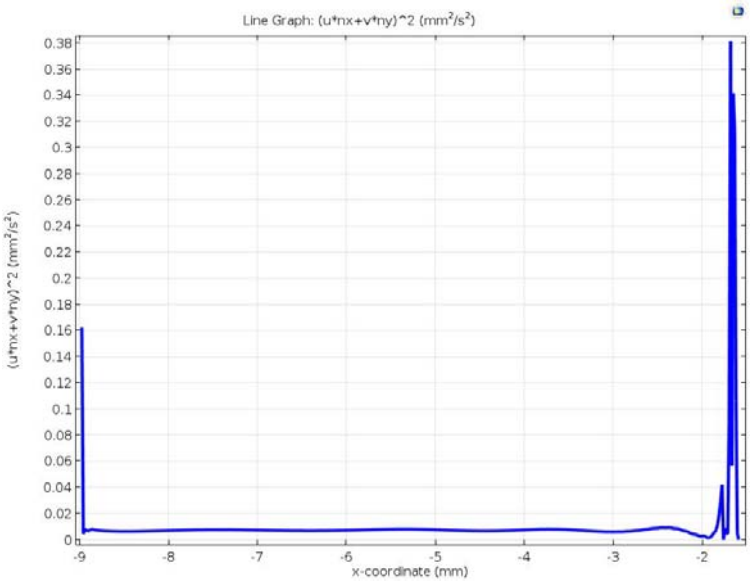

Figure 4. Normal Velocity Profile: Curve A

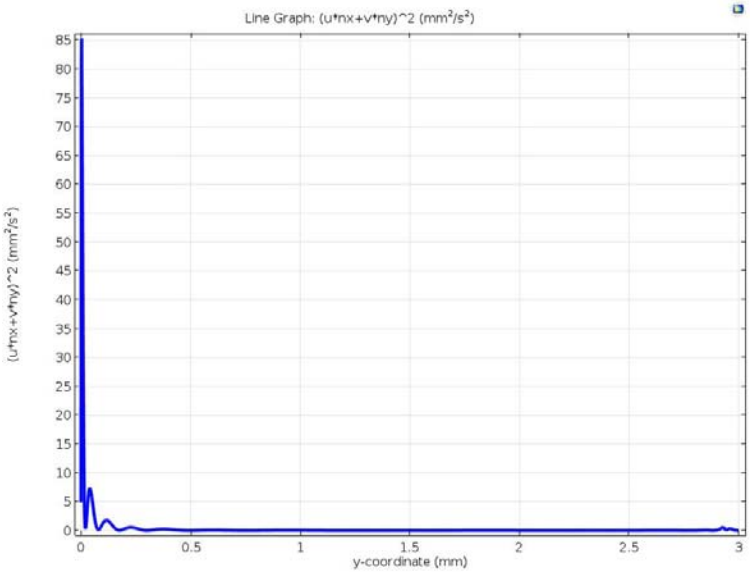

Figure 5. Normal Velocity Profile: Curve B

### *Fiber Orientation Results*

Ten streamlines equally spaced at the flow inlet progress through the flow domain, providing a path for computing fiber orientation tensors. The streamline locations and numbers are shown in Figure 6 which also shows the pseudo-geometry that is defined in Figure 3 representing the optimum extrudate shape. The velocity and velocity gradients are then evaluated along the ten evenly spaced streamlines. These velocity gradients serve as input to Equations 10 and 11, which are then used in Equation 7 to find the local fiber orientation state.

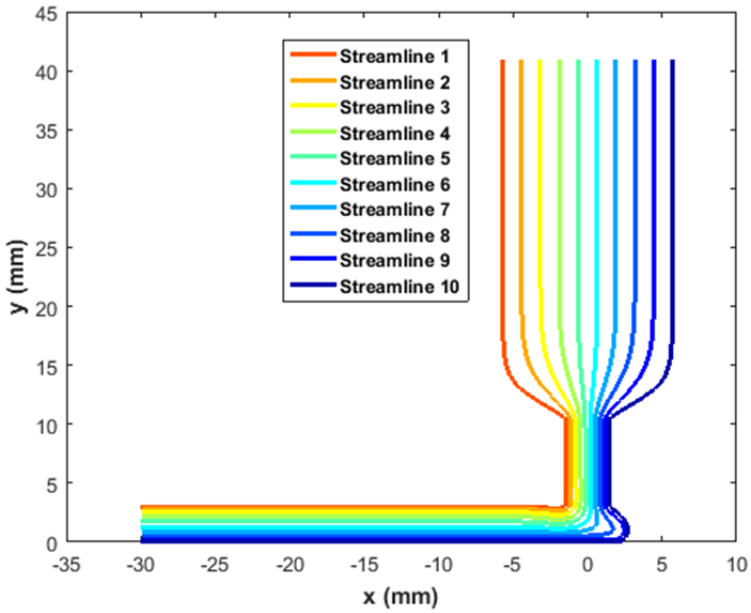

Figure 6. Streamline Plot For Optimum Flow Geometry

Figures 7 and 8 give the fiber alignment in the y and x directions, represented here as $A_{22}$ and $A_{11}$. The degree of fiber alignment for the planar deposition flow can be quantified using the two principle directions computed from the orientation tensors.

It is seen in Figure 7 that the steady state inflow orientation is approximately 0.76 in the y direction which represents a highly aligned state. When the flow enters the convergence zone (d(mm) = 20 to 32) an increase in fiber alignment is seen to increase to a value near 0.9. At $A_{22}$ = 1 uniaxial alignment is achieved therefore the orientation state is very near uniaxial alignment. A small decrease in fiber alignment in the y direction is seen in the straight portion of the nozzle (d(mm) = 32 to 40). This decrease is due to the pure shear flow which attempts to return the fiber alignment state in the y direction to the steady state value shown at the inlet. There is then a substantial decrease in the fiber alignment in the y direction at the nozzle exit. At this point streamlines closest to the upper extrudate curve are showing an increase in velocity as the fluid keeps up with the plate speed. Also, the streamlines close to the leading extrudate curve are slowing down in the eddy area of the flow shown in Figure 3. The flow in this area has velocity gradients that vary substantially and the effect on fiber orientation is therefore expected to vary, but it is seen that the varying velocity gradients serve to quickly and substantially decrease the fiber alignment in the y direction which causes a dramatic increase in the fiber alignment in the x direction. It is assumed that in a three dimensional model some of this effect will be seen in the z direction but in the planar model this effect is seen only in the x direction. The extruded bead exhibits a highly aligned fiber orientation state in the x direction as is shown in Figure 8.

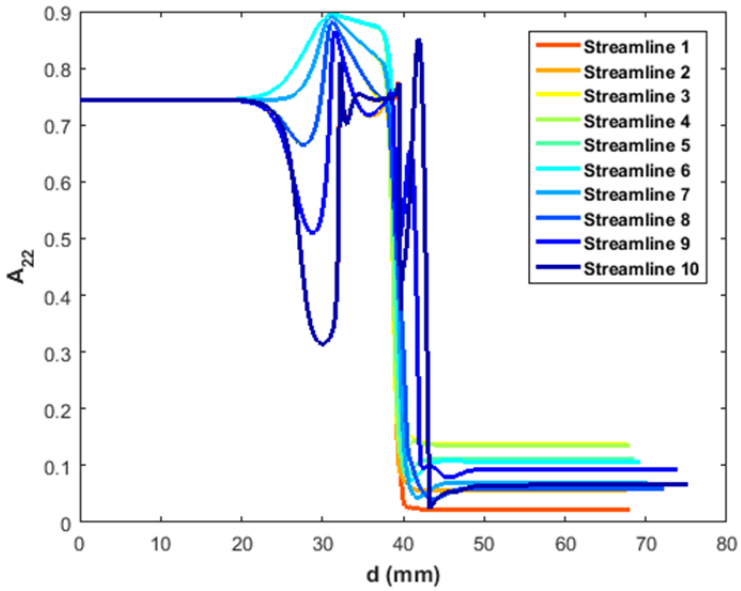


Figure 7. Fiber Alignment in the y Direction, $\mathbf{A_{22}}$

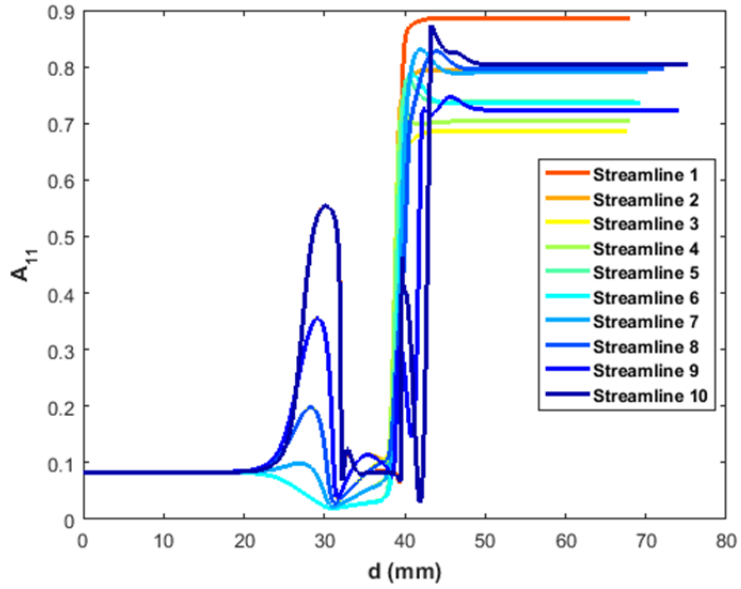


Figure 8. Fiber Alignment in the x Direction, $\mathbf{A_{11}}$

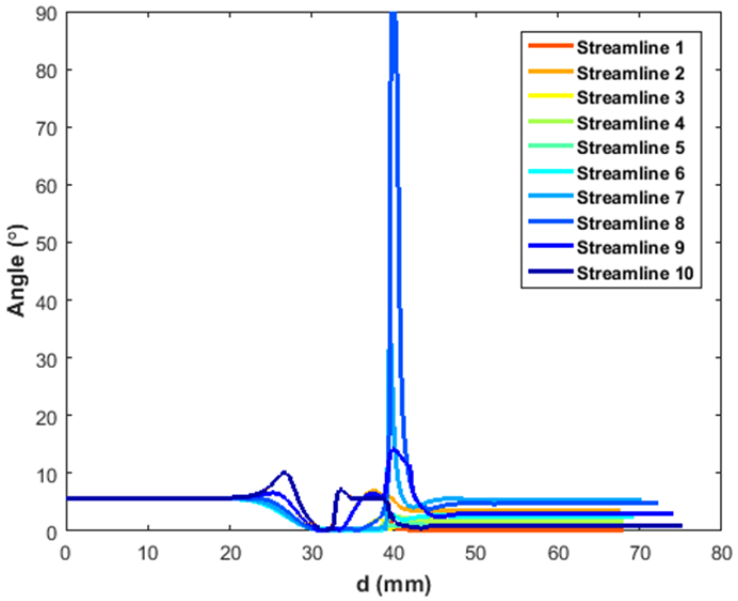

Figure 9. Angle between Eigenvector of Maximum Eigenvalue of $\boldsymbol{A}$ and Normal Velocity Vector

Figure 9 shows the results from the angle between the eigenvector of the max eigenvalue and normal velocity vector study are shown. At the inlet of the nozzle the majority of fibers are aligned within 7 degrees of the unit y vector. In the convergence zone, straight portion of the nozzle, and deposition we see similar results to the previous studies with decreases in angle in the convergence zone, increases in the straight portion, and drastic increases in angle in the deposition portion of the flow. The fiber alignment results shown in Figure 9 show a similar trend to the results from Figures 7 and 8, which is that in the extruded bead the fibers are highly aligned. Computed values of $\gamma$ along all streamlines show that the majority of the fibers are within 5 degrees of the unit x vector which means that the fibers are very highly aligned in the x direction. Another note that should be made relates to the large peak appearing in Figure 9. This peak occurs in the fluid near the recirculation region just below the nozzle exit as seen in Figure 3. The flow transitions from a very fast flow to a very slow flow and finally a fast flow upon deposition. These very quick and substantial changes in the velocity gradients cause a quick and large change in the angle of orientation evaluation as seen in Figure 9 around a value of d = 40 mm.

Figure 10 shows all six independent components of the second order orientation tensor through the bead thickness in the steady state flow after deposition. The fiber orientation tensor components are taken at steady state which is found at x = 25 mm in Figure 3 for y values from 0 to 3 mm through the thickness of the bead. The fiber orientation state in the steady state flow in the deposited bead is no longer changing and the expected values of the bead mechanical properties can be evaluated with the method described previously. After evaluating the mechanical properties of the extruded bead the principal stresses are calculated which appear in Figure 11. Values calculated here include $E_{11}$ and $E_{22}$ which are the longitudinal and transverse modulus of the fiber filled composite that compose the bead. It is seen in Figure 11 that the longitudinal modulus is substantially greater than the transverse modulus which is expected in a highly aligned fiber orientation.

The mechanical properties shown in Figure 11 are evaluated using numerical integration across the thickness of the deposited bead. The values that are calculated from Figure 11 are shown in Table 1. Results show that the longitudinal modulus is almost twice that of the transverse modulus which is expected in a highly aligned fiber filled polymer.

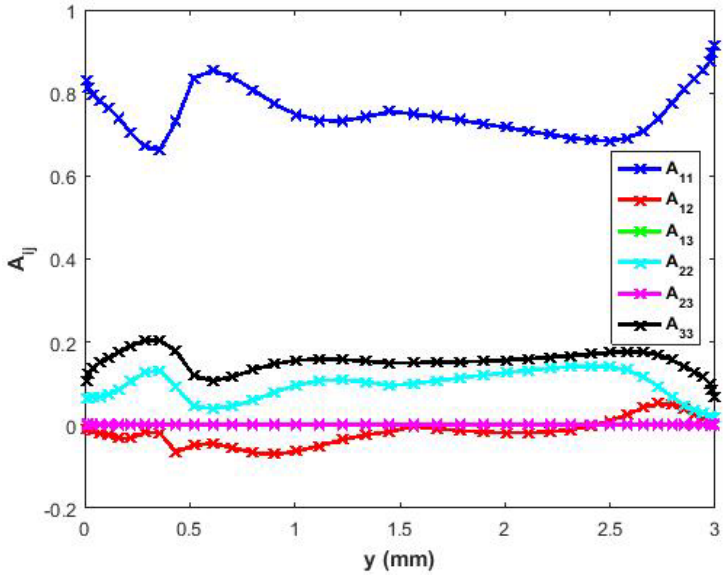

Figure 10. Orientation Tensor Components in Printed Bead

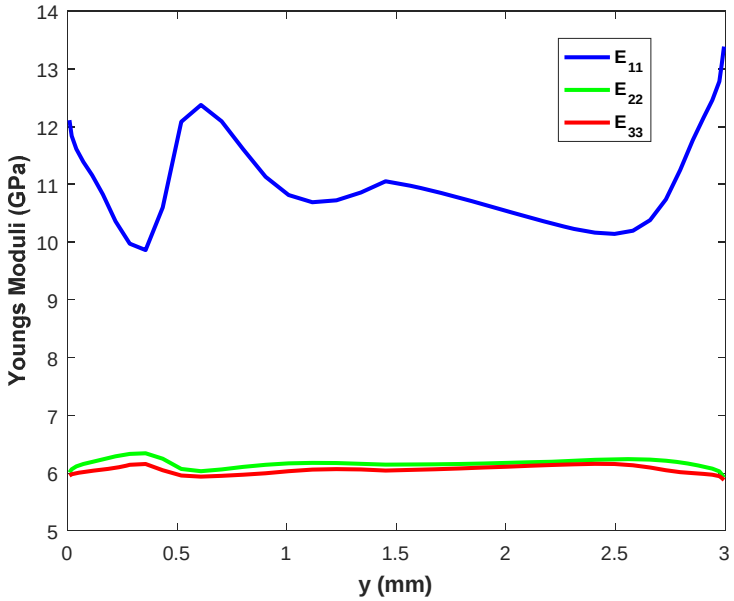

Figure 11. Principal Moduli in the Printed Bead

| Mechanical Properties in Deposited Bead | | |
|---|---|---|
| $E_{11}$ (GPa) | $E_{22}$ (GPa) | $E_{33}$ (GPa) |
| 11.16 | 6.04 | 6.16 |
| $G_{12}$ (GPa) | $G_{13}$ (GPa) | $G_{23}$ (GPa) |
| 2.29 | 2.53 | 2.04 |
| $\nu_{12}$ | $\nu_{13}$ | $\nu_{23}$ |
| 0.15 | 0.47 | 0.31 |

Table 1. Calculated cross section average mechanical properties of the extruded bead

## Conclusions

This paper presents a computational method for evaluating the deposition of short fiber polymer composites for large scale AM systems. An optimization method is presented which computes the shape of the deposition by minimizing the normal velocity of the deposited extrudate. The results presented here are for a single operating condition, however, simulations have been performed using other inputs which have been omitted here for brevity. The fiber orientation was then evaluated for the fiber filled composite using the geometry obtained in the melt flow surface shape optimization. The fiber orientation evaluation shows that fiber alignment in the y direction is high at the inlet, increases in the convergence zone, decreases slightly in the straight portion of the nozzle, and then decreases substantially in the deposition flow after the nozzle exit. The large decrease in the fiber alignment in the y direction occurs as the fiber alignment in the x direction increases which occurs in the region where deposition flow turns below the nozzle exit. Fiber orientation calculations in the deposited bead are calculated to be highly aligned with the principle axis of alignment being within 5 degrees of the longitudinal axis of the bead. The highly aligned fiber state in the beads longitudinal direction results in high longitudinal modulus with a value that is almost twice that of the transverse moduli. It is understood from these results that the expected fiber orientation state in large scale polymer deposition is highly aligned along the bead axis, resulting in a high longitudinal modulus of the deposited bead.

## Future Work

The planar deposition flow model is expected to be improved by using a generalized Newtonian fluid model and by adding the thermal problem to the finite element evaluation. A coupled fiber orientation and flow velocity model is also expected to better represent the actual fiber/fluid flow relationship. These improvements will add to the quality and viability of the fluid model and mechanical properties of the extruded bead.

## Acknowledgements

We would like to acknowledge the financial support of Oak Ridge National Laboratories RAMP-UP 40001455134 and Baylor University during this study. We would also like to thank Strangpresse for the donation of the Model 19 extruder which allows us to evaluate large scale depositon both through lab experiments and fluid modeling approaches.

## References

1. Love, L.J., V. Kunc, O. Rios, C.E. Duty, A.M. Elliot, B.K. Post, R.J. Smith, C.A. Blue, "The Importance of Carbon Fiber to Polymer Additive Manufacturing", Journal of Materials Research, Vol. 29, No. 17, pp. 1893-1898, 2014.
2. Heller, B.P., D.E., Smith, D.A., Jack, "Effects of Extrudate Swell and Nozzle Geometry on Fiber Orientation in Fused Filament Fabrication Nozzle Flow," Journal of Additive Manufacturing, Vol. 12, Part B, pp. 252-264, Oct. 2016
3. Bellini, A. "Fused Deposition of Ceramics: A Comprehensive Experimental, Analytical, and Computational Study of Material Behavior, Fabrication Process and Equipment Design," PhD Thesis, Drexel University, 2002.
4. Jeffery, G.B., "The Motion of Ellipsoidal Particles Immersed in a Viscous Fluid," Proceedings of The Royal Society of London A, Vol. 102 No. 715, pp. 161–179, 1923.
5. Folgar, F., C.L. Tucker III, "Orientatrion Behavior of Fibers in Concentrated Suspensions," Journal of Reinforced Plastic Composites, Vol. 3, No. 2, pp. 98-119, 1984.
6. Advani, S.G., C.L. Tucker III, "The Use of Tensors to Describe and Predict Fiber Orientation in Short Fiber Composites," Journal of Rheology, Vol. 31, pp. 751-784, 1987.
7. Eshelby, J. D., The determination of the elastic field of an ellipsoidal inclusion, and related problems. Proc. Roy. Soc., 1957, A–241, 376–96.
8. Halpin, J. C., Stiffness and expansion estimates for oriented short fiber composites. J. Compos. Mater., 1969, 3, 732–734.
9. Mori, T. and Tanaka, K., Average stress in matrix and average elastic energy of materials with misfitting inclusions. Acta Metallurgica, 1973, 21, 571–574.
10. Lielens, G., Pirotte, P., Couniot, A., Dupret, F., and Keunings, R., Prediction of thermomechanical properties for compression-moulded composites. Composites A, 1997, 29, 63–70.
11. Tandon, G.P., G.J. Weng, "The Effect of Aspect Ratio of Inclusions on the Elastic Properties of Unidirectionally Aligned Composites," Journal of Polymer Composites, Vol. 5, No. 4, pp. 327-333, 1984.
12. Jack, D.A., D.E. Smith, "The Effect of Fiber Orientation Closure Approximations on Mechanical Property Predictions," Composites Part A, Vol. 38, No. 3, pp. 975-982, 2006.
13. Cintra, J.S., C.L. Tucker III, "Orthotropic Closure Approximations for Flow-Induced Fiber Orientation," Journal of Rheology, Vol. 39, No. 6, pp. 1095–1122, 1995.

14. Wetzel, E.D., C.L. Tucker III, “Area Tensors for Modeling Microstructure During Laminar Liquid-Liquid Mixing,” International Journal of Multiphase Flow, Vol. 25, pp. 35-61, 1999.
15. VerWeyst, B.E., C.L., Tucker, “Fiber Suspensions in Complex Geometries: Flow-Orientation Coupling,” The Canadian Journal of Chemical Engineering, Vol. 80, pp. 1093–1106, 2002.
16. Tucker III, C.L., E. Liang, “Stiffness Predictions for Unidirectional Short-Fiber Composites: Review and Evaluation,” Composites Science Technology, Vol. 59, No. 5, pp. 655–671, 1999.